



A Clean Process for the Recovery of Potash Fertilizer from Glauconitic Rock via Hydrogen Gas Pre-treatment and Mild Acid Leaching

SAURABH SHEKHAR,¹ V. KUMARI,² S. SINHA,¹ D. MISHRA,¹
and K.K. SAHU^{1,3}

1.—CSIR-National Metallurgical Laboratory, Jamshedpur 831007, India. 2.—Indian Institute of Science Education and Research, Bhopal 462066, India. 3.—e-mail: kksahu@nmlindia.com

Potassium (K) is an essential macronutrient for the healthy growth and development of crops but their conventional resources are only limited to a few countries. Deficiency of potash fertilizer in soil is a widespread problem for countries with no such potash deposits to meet the present as well as future food demands. In view of this, the present work investigates a novel interdisciplinary approach for the recovery of potash fertilizer from widely available glauconitic rocks. The rock sample containing ~ 6–8% K₂O can be considered a potential alternative source of K-fertilizer. The characterization study revealed that the quartz, glauconite and K-feldspar are the major mineral phases, and the glauconite occurs in the form of ovoidal-shaped pellets. As potassium is trapped between di-octahedral T-O-T stable structure of glauconite, a combined process involving hydrogen gas reduction followed by mild hydrochloric acid leaching was developed to enhance the effective recovery of potassium. More than 99% of potassium dissolution was achieved with 20% (v/v) hydrochloric acid leaching at 80°C for the sample reduced at 500°C in the presence of 20 mL/min of H₂ gas flow rate for 2 h. The leach liquor was further treated to recover potassium as muriate of potash (MOP).

INTRODUCTION

The exponential increase in world's population has created several challenges including the food demand. To ensure present as well as future global food security, a huge amount of fertilizer is needed to increase the crop yield.^{1–3} This increase in crop production to overcome the food security challenges has to come from the available agriculture land, which is only 11% of globe's total land surface, with no scope for further expansion due to rapid urbanization.^{4–6} Recently, studied nutrient budgets claim that among the principal fertilizers (N, P and K), the off take of potassium (K) from soil during crop production greatly exceeds the inputs whereas nitrogen (N) and phosphorous (P) are roughly in balance state.^{7–9} Therefore, to maintain constant

nutrient status of potash fertilizer, the worldwide production of potassium needs to be doubled or tripled to increase both the quality and quantity of food grains.^{10–13}

The global demand for potassium (K₂O) is increasing with a growth rate of nearly 2.5–2.8% per annum, and it is projected to reach > 50 million tons by 2030.^{14–17} At present, the world's conventional potassium resources are mainly available as marine evaporative bedded salt deposits such as sylvinite, langbeinite, carnallite, kainite and Dead Sea brines. Over 90% of these potash deposits are concentrated in only ten countries;^{2,18,19} other places like India, Europe and Africa do not have such deposits and are already reported to be K deficient.^{20,21} Considering the continuous increase in potash demand and uncertainties in its future supply, there is an urgent need for an investigation of locally available alternate resources to potassium in order to maintain self-sufficiency.^{22–24} The availability of K-bearing silicate minerals such as K-

feldspar, nepheline syenite, biotite, muscovite, phlogopite and glauconite, with considerable amounts of K_2O , i.e., 5–15%, has now attracted the attention of researchers as an alternative source for potash fertilizer.^{22,25–27} Among these silicate minerals, glauconite is considered a potential source of potash fertilizer because of its poor structural organization, occurrence in granular form, susceptibility to weathering and worldwide distribution.^{23,24,28,29}

Glauconite belongs to a group of naturally occurring, compositionally heterogeneous, dioctahedral, potassium, iron-rich micaceous clay minerals with a generalized chemical formula of $(K, Na, Ca)(Fe^{3+}, Fe^{2+}, Al, Mg)_2(Al, Si)_4O_{10}(OH)_2 \cdot nH_2O$. The structure of glauconite consists of two tetrahedral sheets facing one octahedral sheet with interlayer K^+ cations. However, most of the potassium is trapped in the crystal lattice of tetrahedral-octahedral-tetrahedral (T-O-T) structure of the mineral. Direct application of glauconite in soil after size reduction and physical beneficiation cannot be implemented in the mainstream of agriculture because of very slow release of potassium.^{12,13,30,31} Therefore, various methods have been studied and developed for efficient release of potassium and its recovery in the form of soluble salts. These methods mainly include bio-leaching,^{32,33} direct and additive-assisted leaching.^{34–38} Other common methods studied to recover potassium include direct roasting and roasting in presence of additive followed by acid or water leaching.^{39–41} It is evident from the above literature that most of these processes target silica and alumina to break the stable structure, which requires very aggressive treatment condition such as very fine grinding, high acid or alkali concentration, use of hazardous and corrosive salt, high alkali-to-solid ratio, and higher roasting and leaching temperature. Apart from this, reports on these processes are limited to potassium dissolution and do not discuss its downstream processing for its recovery as a final product. The current authors in their previous work^{42,43} attempted to target iron present in the glauconite structure as a weak link to break the matrix through reduction roasting in presence of coke. The process was found to be efficient, and it was possible to recover 98.77% of K with 30 vol.% HCl at 80°C for the sample reduced at 700°C in the presence of 10 wt.% coke. Use of coke for reduction roasting generates CO and CO_2 , which will consequently increase the carbon footprint. Considering this challenge, H_2 gas was used instead of coke in the present work as a clean source for the reduction roasting of glauconite to break the structure and to release potassium effectively. The advantage of using H_2 over the carbon source is that the rate of diffusion for H_2 is four times that of the CO, and the partial pressure of water helps in increasing the reduction rate.^{44,45} This developed process is ecofriendly as the final product of H_2 reduction is water (H_2O). This process helped to achieve higher potassium dissolution at relatively

lower reduction temperature and acid concentration, making it more economical compared to the earlier studied process.

In this work, we have investigated the effect of various operating parameters on the potassium dissolution from glauconitic rocks through reduction roasting in the presence of H_2 gas followed by acid leaching and crystallization of the leach liquor after purification. In addition, complementary studies have been carried out using thermodynamic modeling of reduction roasting with the help of FactSage 6.4 coupled with XRD to understand the pathway through which reactions occur. The results of this study could lay the groundwork for the development of a novel and clean process to extract potassium from Indian glauconitic rock to produce fertilizer-grade potassium chloride (muriate of potash) for agricultural application.

EXPERIMENTAL SECTION

Materials and Reagents

The glauconitic rock sample used in this research work was collected from Kutch district, Gujrat, India. The run of mine sample was crushed and ground $< 425 \mu m$ for pre-treatment and leaching studies. A representative sample was taken out after conning and quartering and was further ground $< 75 \mu m$ for analytical testing. The mineral phases and chemical composition of the rock sample were analyzed by X-ray diffraction (XRD) and wet chemical as well as instrumental methods, respectively, and the results are presented in Table I and Fig. 1.

The rock predominantly contains 5.87% K_2O and 17.56% Fe_2O_3 as the major metal component, and the contents of main impurities are 56.38% SiO_2 and 5.93% Al_2O_3 . The XRD patterns of powdered rock sample (Fig. 1) confirm the presence of quartz (JCPDS 83-1604), glauconite (JCPDS 02-0466) and K-feldspar (JCPDS 86-0437) as major mineral constituents. All the chemical reagents used in this study were of analytical grade, obtained from Merck, Germany, and used directly without any further purification. Hydrogen gas used as a reducing agent was of XL grade with 99.999% purity obtained from Linde India, Ltd. Double-distilled water having conductivity $< 0.1 \mu S cm^{-1}$ was used throughout the experimental work.

Methodology

Hydrogen Gas Pre-treatment

The ground sample below $425 \mu m$ was thoroughly mixed with water, and the mixture was pelletized to make pellets of 10–12 mm diameter. The reduction roasting experiments were carried out in a horizontal tube furnace, and the furnace temperature was monitored using a Cr/Al (K, Type) thermocouple equipped with PID digital controller (Yudian, Hong Kong). A rotameter is attached to the furnace to

Table I. Chemical composition of raw glauconitic rock sample (wt.%)

Composition:	SiO ₂	Fe ₂ O ₃	Al ₂ O ₃	K ₂ O	MgO	FeO	TiO ₂	CaO	P ₂ O ₅	LOI
Content (%):	56.38	17.56	5.93	5.87	2.35	1.10	0.88	0.56	0.39	8.71

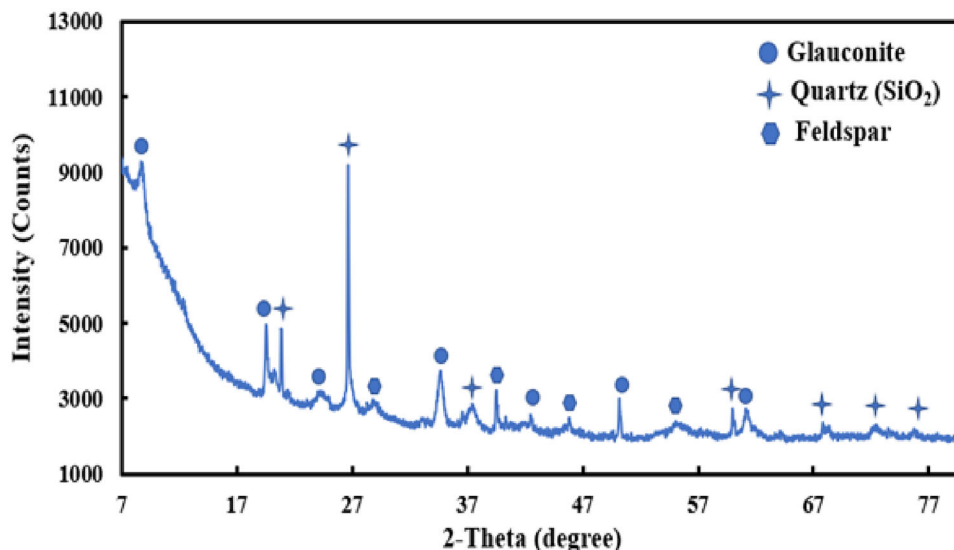


Fig. 1. XRD pattern of powdered glauconitic rock sample.

measure the gas flow rate. The schematic diagram of the reduction roasting apparatus is provided in supplementary Fig. 1. Initially, the tube furnace was heated to a set temperature, and an alumina crucible loaded with pellets was kept into the hot zone for a fixed time interval. The furnace was first purged with nitrogen for 5–10 min to ensure inert atmosphere followed by hydrogen gas purging for desired time. After roasting, the furnace was allowed to cool below 100°C. The reduced pellets were taken out and ground below $-425\ \mu\text{m}$ in a mortar pestle and subsequently subjected to acid leaching study.

Leaching Process

Leaching experiments were performed using a three-neck closed-type glass reactor of variable volume placed on a ceramic top hot plate with an inbuilt digital temperature controller and a magnetic stirrer. A reflux condenser was attached to the flask to prevent evaporation losses. A certain volume of hydrochloric acid of desired concentration was mixed with water to prepare a leaching solution. A weighted amount of the sample was added to the leaching solution to maintain constant pulp density (PD) of 100 g/L with a constant stirring rate of 300 rotations per minute (rpm) for 2 h. The pregnant liquor obtained after leaching was filtered with the help of a pressure filtration unit followed by washing with deionized water. The pregnant liquor and filter cake were separately collected and

analyzed to determine the metal contents in them. The leaching efficiency (%L) of metals is defined as the amount of metal leached to the acidic solution over the initial amount of metal present in the pretreated sample.

$$\%L = \frac{V_{aq}[M]_{aq}}{m}$$

where $[M]_{aq}$ (mg/L) is the metal concentration in the leachate after leaching, V_{aq} is the volume of the leachate, and m represents the initial metal mass present in the sample. To check the repeatability of experimental data, all experiments were performed in triplicate, and their average value was reported.

Evaporative Crystallization

The acidic leach solution containing potassium and iron as a major element was first treated to separate iron followed by evaporation of potassium-containing solution. The evaporation of the liquor was carried out in an open beaker at 80°C. During evaporation, the solution was supersaturated, that is, the salt concentration in the solution exceeds its solubility limit in water; then, the nucleation of the KCl crystal was started. After crystallization, the slurry was immediately filtered under vacuum, washed with ethanol and dried at 60°C for 8–10 h in an electric oven. The KCl crystals were further characterized by using XRD and SEM-EDS.

Analysis and Characterization

Thin sections of glauconitic rock sample were prepared and observed under a petrological microscope for mineralogical and textural characterization of rock samples. The method for preparation of thin sections is described elsewhere.²⁴ The microscopic analysis was carried out using a Leica DM 4500P polarizing microscope (Chiyoda-ku, Japan) with an attached Leica DFC420 camera. The microstructure picture and energy spectrum analysis results of the rock were performed by using Zeiss Evo 18 scanning electron microscopy (SEM) (Oberkochen, Germany) attached to an energy-dispersive X-ray spectroscopy (EDS) whereas the leach residue and final product were analyzed through FEI Nova NanoSEM 430. The chemical composition of the rock was determined by X-ray fluorescence spectroscopy (XRF) (Bruker SRS 3400, Germany), Thermo-Scientific iCE3000 series atomic absorption spectroscopy (AAS) and inductively coupled plasma optical emission spectroscopy (ICP-OES; Agilent, USA) after tri-acid digestion of the representative sample. The phases of raw as well as pre-treated sample were analyzed by X-ray diffraction (XRD) under the condition of 2θ range of 5° to 80° at a scanning rate of $1^\circ/\text{s}$ with a step of 0.02° using a Bruker D8 Discover diffractometer (Bruker, Germany) with Cu $K\alpha$ radiation. The XRD measurement for the final product was done in 2θ range from 15° to 80° . The thermo-gravimetric (TG) and differential thermal (DTA) data were analyzed in argon atmosphere from 25°C to 1000°C at the heating rate of 10°C per min using LECO 701 (Michigan, USA). The pH of the solution was measured with Mettler Toledo SevenExcellence pH meter with an attached Inlab Expert Pro ISM electrode (Greifensee, Switzerland).

RESULTS AND DISCUSSION

Petrographic and Morphological Analysis

Petrographic observation shows that the glauconitic rock sample is fine grained and primarily composed of quartz (45–50%), glauconite (30–35%) and K-feldspar (15–20%) calculated by using point counting method as shown in Fig. 2a and b. The sample contains both monocrystalline and polycrystalline, sub-angular to sub-rounded quartz, which is the major siliciclastic component of the sample (Fig. 2b).

Iron oxide is present in a small amount in the sample and occurs as irregular patches (Fig. 2d). Glauconite is the second major component of the sample after quartz, which is yellowish green to dark green in color (Fig. 2a, b, c and d). Glauconite mainly occurs as oval and rounded pellets of variable size ranging from $100\ \mu\text{m}$ to $200\ \mu\text{m}$ (Fig. 2c). The sub-angular to sub-rounded glauconite pellets are mostly oval, but a few grains are elongated and irregular in shape, indicating the evolved nature of

glauconite. Glauconites show faint pleochroism and high second-order interference color under the microscope (Fig. 2a and b). Fractured and broken pellets are present in the sample (Fig. 2c and d). The presence of fractures is indicative of the in situ formation of glauconite. The backscattered SEM image of the rock shows that glauconite particles are present in the form of pellets (Fig. 3a). These pellets show variation in size, which ranges from approximately $100\text{--}200\ \mu\text{m}$. Morphology of pellets is variable, ranging from spheroidal to ovoidal with cracks (Fig. 3a). Small blades ($0.5\text{--}1\ \mu\text{m}$ in size) of random orientation were observed under the SEM, which is referred to as the 'rosette' structure (Fig. 3b). This particular micro-texture is indicative of the evolved nature of glauconite. The EDS spectrum of pellets shows Si, Fe, K, Al, Mg, Ca and Ti as their possible constituents, and concentration of these major elements (semi-quantitative estimation) is typical of glauconite (Fig. 3c).

Thermal Behavior Studies

The effect of temperature on the rock sample was assessed by thermogravimetry in the range of 24°C to 1000°C . The obtained TG-DTA profile is provided in Supplementary Fig. 2. The TG data showed three major temperature ranges for mass loss. The weight loss $< 200^\circ\text{C}$ was associated with absorbed water, whereas between 200°C and 400°C was due to hydration water. The weight loss above this temperature occurred because of dehydroxylation and led to the removal of structural water. The endotherms below 200°C represented expelling of surface and interlayer water molecules, whereas the exotherm around 400°C was observed because of the oxidation of ferrous iron to the ferric state along with some contribution from oxidation of organic matter.

Direct Dissolution Studies Before Pretreatment

To bring potassium in leach solution for its recovery as soluble salt, the as-received sample was first leached with water. The potassium dissolution was only 600 ppm with water leaching at 80°C for 4 h of leaching time. The results show that the potassium is not present in water soluble form. Therefore, the sample was treated with hydrochloric acid to recover potassium in the form of chloride salt, i.e., muriate of potash (KCl). Leaching study of raw sample was carried out by varying the acid concentration in the range 10–30% (v/v) and the leaching temperature from 30°C to 80°C .

The pulp density and leaching time were kept constant at 10% and 2 h, respectively (Fig. 4). Upon increasing the HCl concentration and leaching temperature, the dissolution of potassium increased but the extent of potassium dissolution was very poor. A maximum dissolution of 20.7% potassium was achieved at 80°C with 30% HCl concentration.

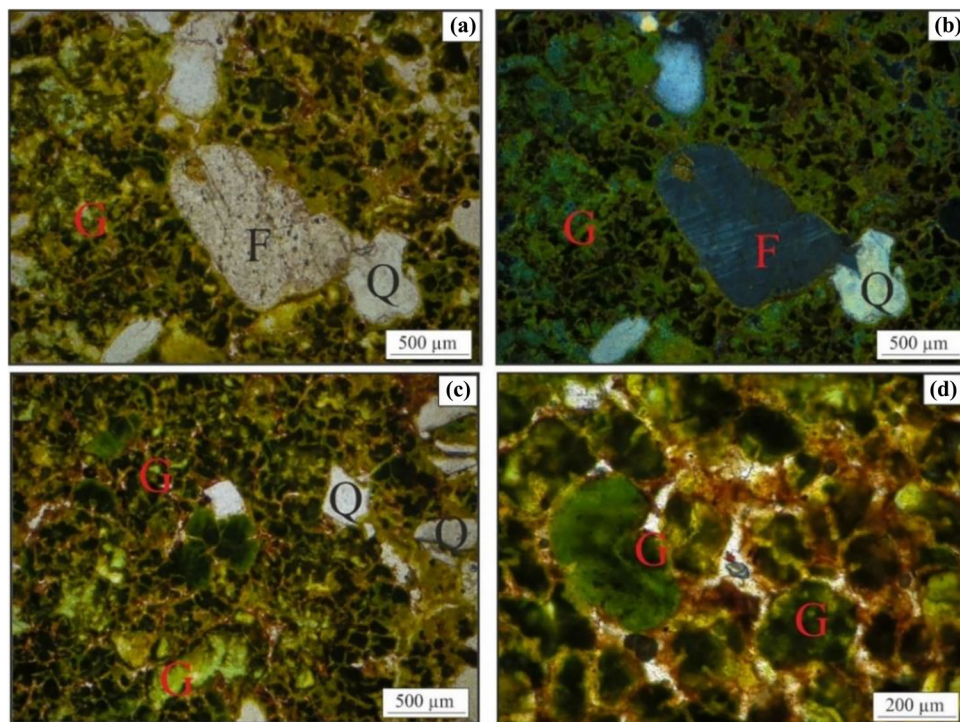


Fig. 2. Photomicrograph of the glauconitic rock sample (a) under plane polarized light (PPL) and (b) under cross-polarized light (XPL) showing the glauconite pellets (G) and grains of quartz (Q) and K-feldspar (F) are mainly microcline. Fractured and broken glauconitic pellets (c-d) show variation in the morphology from oval to irregular (c-d) under plane polarized light (PPL).

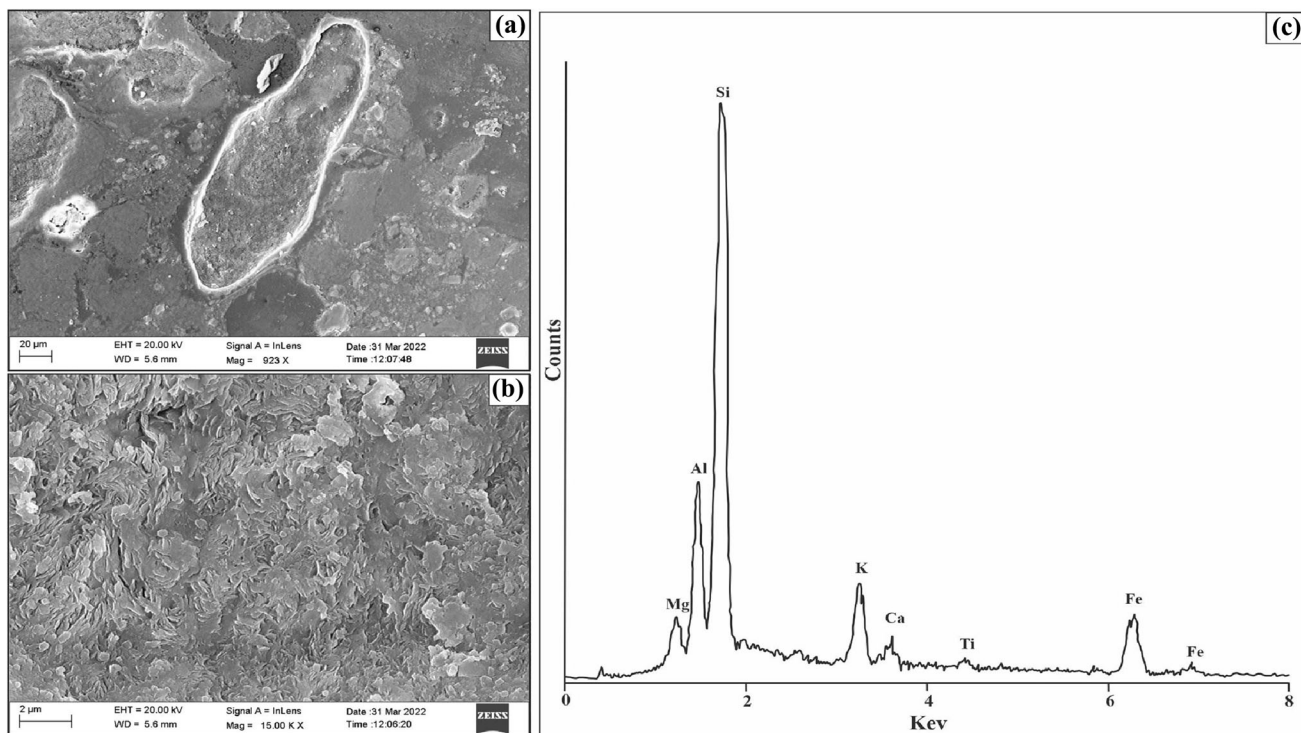


Fig. 3. SEM micrograph of glauconite showing (a) morphology of pellet; (b) internal structure (micro texture) of glauconitic pellet; (c) EDS spectrum of glauconitic pellets.

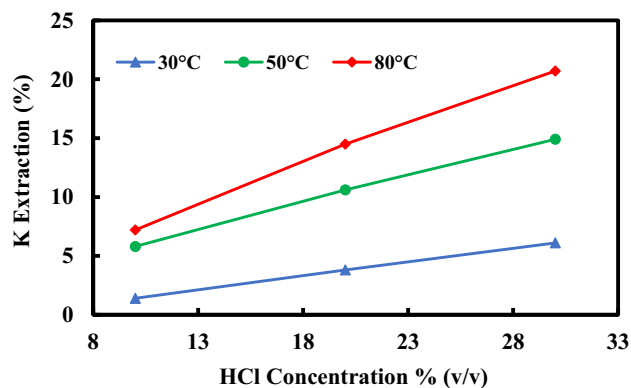


Fig. 4. Extraction of potassium against HCl concentration at different leaching temperatures (leaching time: 2 h, PD: 100 g/L, stirring speed: 300 rpm).

The above result showed that the potassium is not present in the form of exchangeable ions with H^+ within the glauconite structure. Further increase in HCl concentration only leads to a marginal increase in the potassium dissolution along with generation of highly acidic leach solution, which will create a problem with downstream processing for the recovery of potassium in the form of soluble chloride salt.

Role of Pre-treatment

The above results show that some pretreatment is required to make potassium amenable to leaching from the stable matrix of glauconite. To determine the kind of pre-treatment required to break the stable structure, we identify iron as a weak link within the glauconite crystal structure. Most of the octahedral sites were occupied by iron in the form of Fe^{3+} . The oxidation state of the iron can be easily altered. Therefore, an attempt was made in this work to reduce Fe^{3+} to Fe^{2+} in the presence of reducing gas (H_2) to break the stable structure. The change in oxidation state led to the distortion in the structure as the element attempted to compensate for the increased size of the Fe^{2+} ions. The reduction of Fe^{3+} to Fe^{2+} produced a net increase of negative surface charge on the structure, which enabled increasing proton attraction during HCl leaching. The surface area, porosity, volume and pore size of glauconite structure significantly increased, which will help in easy and fast diffusion of H^+ to extract K^+ even under mild acid leaching.

Optimization of Pre-treatment and Leaching Parameters

To determine the optimized condition for H_2 gas reduction followed by HCl leaching, process parameters like reduction temperature, gas flow rate, leaching temperature and acid concentration were studied and analyzed. Efficiency of these parameters was calculated based on percent dissolution of potassium after acid leaching. All the reduction experiments were carried out on a ~ 100 -gm scale

Table II. Effect of H_2 gas flow rate on percent extraction of K

Amount of H_2 gas flow rate (mL/min)	% K extraction
10	54.65
15	68.23
20	79.40
25	80.20

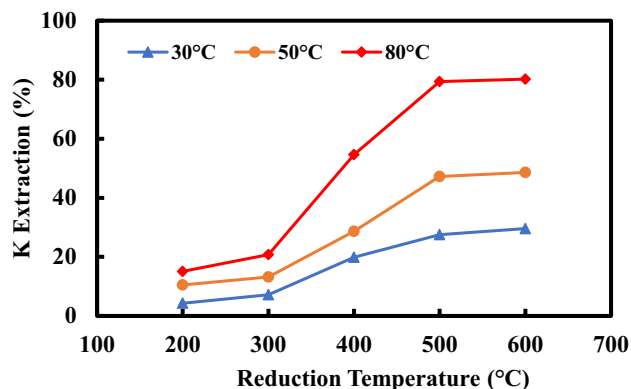


Fig. 5. Extraction of potassium against reduction and dissolution temperature (H_2 flow rate: 20 mL/min, reduction time: 2 h, HCl conc.: 15%).

within the temperature range of 200–600°C at a fixed time interval of 2 h. The effect of H_2 gas flow rate on percent extraction of potassium was investigated from 10 mL/min to 25 mL/min at reduction temperature of 500°C, HCl concentration of 15% (v/v) and leaching temperature of 80°C for 2 h of leaching time. The results were presented in Table II.

The extraction of potassium was 54.65% to 79.40% when the H_2 flow rate increased from 10 mL/min to 20 mL/min. The extraction efficiency of potassium increased with an increase in H_2 flow rate and reached an almost constant value after 20 mL/min of flow rate. However, a further increase in H_2 gas flow rate (25 mL/min) did not show any significant increase in potassium dissolution (80.20%). Therefore, the optimum flow rate was determined to be 20 mL/min of H_2 gas for further sets of experiment. The effects of reduction (200–600°C) and leaching temperature (30–80°C) on percent extraction of potassium at H_2 gas flow rate of 20 mL/min with HCl concentration 15% (v/v) for 2 h of leaching are shown in Fig. 5.

The results showed that the reduction and leaching temperature both had a significant effect on dissolution of potassium. At lower reduction temperature ($< 300^\circ C$), the potassium dissolution was very poor because of incomplete reduction of Fe^{3+} to Fe^{2+} . When the reduction temperature increased from 200°C to 500°C, the extraction efficiency of

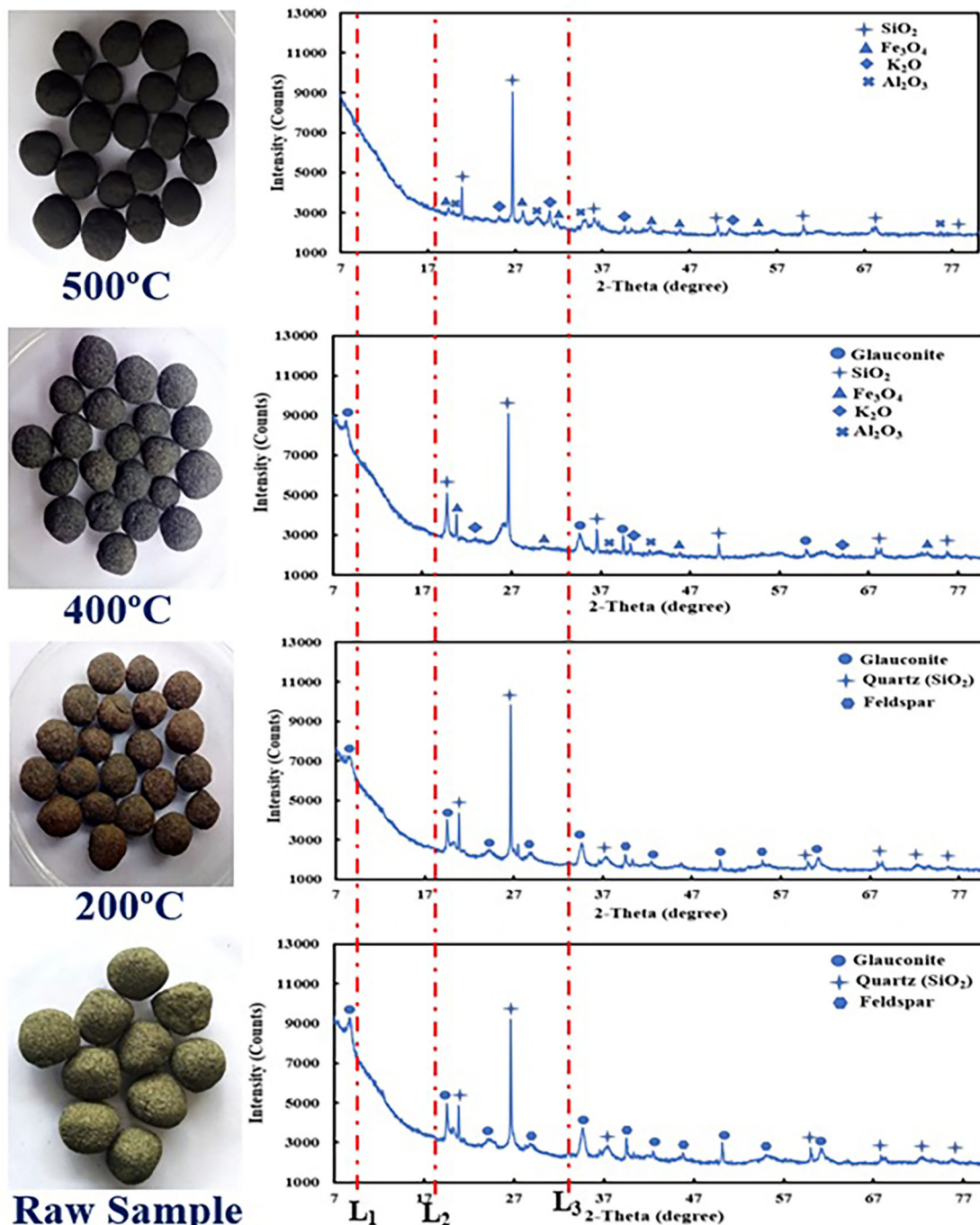


Fig. 6. Comparison of XRD patterns of glauconitic sample reduced at different temperatures (200°C, 400°C and 500°C) with respect to raw sample.

potassium increased from 10.5% to 47.2% at 50°C leaching temperature. A further increase in reduction temperature from 500°C to 600°C showed only a marginal increase in the dissolution of potassium. Increasing the leaching temperature from 30°C to 80°C at reduction temperature of 500°C caused the extraction percent of potassium to increase from 27.5% to 79.4%. This increase in potassium

dissolution can be explained by a decrease in viscosity of lixiviant with leaching temperature, and the glauconite structure completely collapsed at 500°C of reduction temperature. We tried to explain this reduction roasting mechanism using comparative XRD analysis. The XRD pattern of the reduced sample at different temperatures was examined and compared with that of the raw sample (Fig. 6). An

increase in reduction temperature shows that the intensity of glauconite phase goes on decreasing with simultaneous appearance of various new phases, which is reflected by the change in color of pellets from green to brown and finally black. The major XRD peaks of glauconite at 10.10 Å, 4.53 Å and 2.58 Å continued to decrease with the increase in temperature from 200°C to 500°C and completely

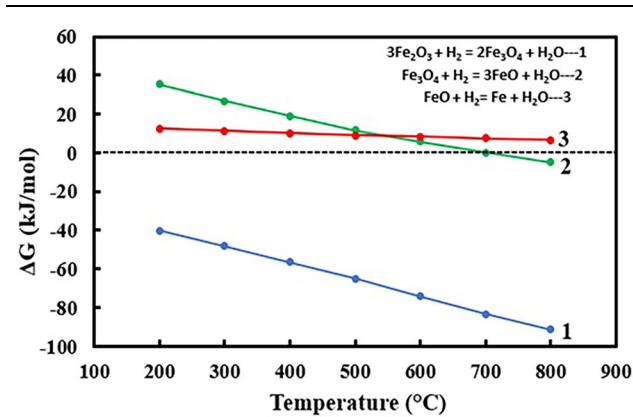


Fig. 7. Thermodynamic graph of Gibbs free energy as a function of temperature for H_2 reduction.

Table III. Effect of HCl concentration on percent extraction of K

HCL concentration % (v/v)	% K extraction
05	32.5
10	65.3
15	79.4
20	99.3
25	99.8

disappeared at 500°C, as shown by vertical lines L1, L2 and L3 (Fig. 6). The appearance of new peaks mainly includes magnetite (Fe_3O_4), potassium oxide (K_2O) and aluminum oxide (Al_2O_3) along with quartz (SiO_2).

The feasibility of reactions forming the various iron oxide phases during reduction roasting was further studied using FactSage 6.4. thermochemical software (Fig. 7). The results show that the value of Gibbs free energy change (ΔG) for the formation of Fe_3O_4 from Fe_2O_3 in presence of H_2 gas (reaction 1) is feasible throughout the temperature range between 200°C to 600°C, whereas the formation of FeO (reaction 2) is feasible above 700°C. The conversion of FeO to metallic iron (reaction 3) requires a reduction temperature $> 1000^\circ C$.

Lastly, the HCl concentration needs to be optimized for potassium extraction, so it was varied within the range of 5% (v/v) to 25% (v/v) at reduction temperature of 500°C at 80°C for 2 h as given in Table III. The leaching results indicate that the dissolution of potassium increased from 32.50% to 99.35% with an increase in HCl concentration from 5% to 20% (v/v). A further increase in acid concentration resulted in a marginal increase in dissolution of potassium. A maximum of 99.35% potassium dissolution was achieved at the above optimized conditions.

XRD and SEM-EDS Analysis of Leach Residue

The leach residue obtained after leaching of pre-treating sample at optimized condition was analyzed using XRD and SEM-EDS. The XRD peaks (Fig. 8a) clearly show that the residue was mainly composed of quartz (SiO_2), and the other mineralogical phase included aluminum oxide (Al_2O_3). The SEM image (Fig. 8b) showed that the surface of quartz grains is smooth with sharp edges. However, some particles are rough and irregular in shape

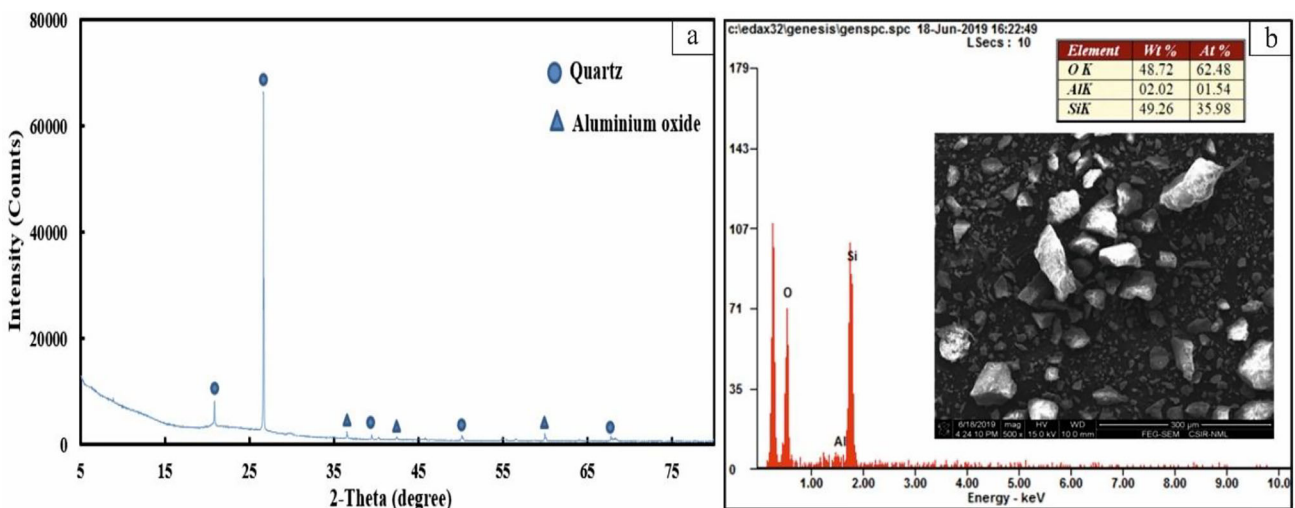


Fig. 8. (a) XRD diffractogram and (b) SEM-EDS analysis of leach residue.

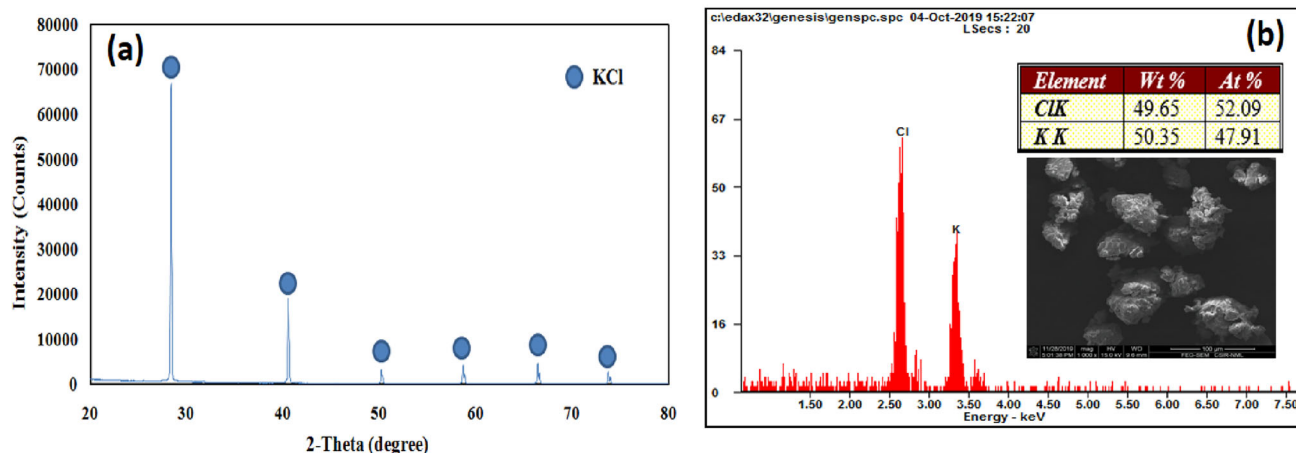


Fig. 9. (a) XRD pattern and (b) SEM-EDS analysis of synthesized KCl.

representing aluminum oxide. The area EDS analysis shows that the residue is mainly composed of Al (2.02 wt.%), Si (49.26 wt.%) and O (48.72 wt.%), which is consistent with the XRD interpretation.

Product Recovery and Characterization

Finally, the dissolved potassium needs to be recovered as a final product in the form of sylvinit (KCl), and a sufficient amount of leach liquor needs to be generated. Therefore, ~ 250 g of sample was treated at optimized condition; therefore, the leach solution with 11.8 g/L of K was obtained after single-stage leaching. The simultaneously dissolved iron (30.3 g/L) was present in the form of Fe^{2+} , which was first oxidized to Fe^{3+} by adding a measured amount of H_2O_2 at room temperature under continuous stirring for 15–20 min. The Fe^{3+} was then separated through solvent extraction with a solvent system consisting of 20 vol.% Aliquat 336 and 15 vol.% TBP, showing almost 99.96% extraction of iron in two stage at O:A ratio of 1:0.75. The stripping efficiency was 99.95% with 0.05 M HCl in three stages at O:A ratio of 0.4:1, as described elsewhere⁴³ in detail, which could be further treated to recover it as high-value iron oxide nanoparticles. The potassium containing final liquor (raffinate) obtained after solvent extraction was evaporated till the start of crystal formation and slowly cooled to about 20°C to obtain KCl crystals.

The white crystal formed was filtered, dried and powdered for XRD and SEM-EDS analysis to check its purity. The XRD peak of potassium chloride salt (Fig. 9a) was consistent with JCPDS file no. 72-1540, which indicates that the synthesized sylvinit is of high purity. The SEM-EDS analysis (Fig. 9b)

shows irregularly shaped, agglomerated KCl particles with elemental distribution corresponding to 50.35% K and 49.65% Cl, which are very close to the theoretical values (K: 52.45; Cl: 47.55). The potassium chloride crystal thus obtained was found to be $> 98\%$ pure and suitable for fertilizer application. The complete flowsheet of developed process is provided in Supplementary Fig. 3.

CONCLUSION

An innovative process was developed to recover potassium as muriate of potash (KCl) from glaucanitic rock containing 5.87% K_2O , 56.38% SiO_2 , 17.56% Fe_2O_3 and 5.93% Al_2O_3 as major constituents. The physico-chemical characterization of the rock revealed that it is predominantly composed of quartz, K-feldspar and oval to sub-rounded shape glaucanite pellets of 100–200 μm size. The preliminary investigation revealed that the potassium was locked within stable aluminosilicate matrix (T-O-T) of glaucanite structure. Direct acid leaching of the raw sample resulted in dissolution of only 20.7% potassium with 30% (v/v) HCl at 80°C for 2 h. To maximize the potassium dissolution, a novel and clean process was developed to rupture the stable structure. The developed process comprises pretreatment of glaucanitic rock with hydrogen gas followed by mild hydrochloric acid leaching. Reduction roasting in presence of H_2 gas with flow rate of 20 mL/min at 500°C for 2 h showed a direct effect on potassium dissolution as the glaucanite structure was completely collapsed. The leaching of reduced sample with 20% (v/v) HCl at 80°C for 2 h resulted in the dissolution of 99.35% potassium. The simultaneously dissolved iron was separated through

solvent extraction,⁴³ whereas the raffinate was crystallized to produce potassium chloride. The XRD and SEM-EDS study of the final product confirms its suitability as potash fertilizer.

SUPPLEMENTARY INFORMATION

The online version contains supplementary material available at <https://doi.org/10.1007/s11837-024-06539-w>.

ACKNOWLEDGMENTS

The authors sincerely thank the Director, CSIR-National Metallurgical Laboratory, for his permission to publish this work. Authors also thank Dr. P.R. Golani and Mr. Hajaj Basheer from Geological Survey of India (GSI) for providing the sample.

CONFLICT OF INTEREST

The authors declare that they have no conflict of interest.

REFERENCES

- D. Ciceri, D.A.C. Manning, and A. Allamore, *Sci. Total Environ.* 502, 590 <https://doi.org/10.1016/j.scitotenv.2014.09.013> (2015).
- S. Prakash and J.P. Verma, Global perspective of potash for fertilizer production, in *Potassium solubilizing microorganisms for sustainable agriculture*, vol 327. ed. by V. Meena, B. Maurya, J. Verma, and R. Meena (Springer, New Delhi, 2016). https://doi.org/10.1007/978-81-322-2776-2_23.
- Q. Ma, R. Bell, C. Scanlan, and A. Neuhaus, *Crop Pasture Sci.* 73, 981 <https://doi.org/10.1071/CP21612> (2022).
- R.A. Rawashdeh and P. Maxwell, *J. Resour. Policy* 41, 143 <https://doi.org/10.1016/j.resourpol.2014.05.004> (2014).
- D. Dmitrieva, A. Ilinova, and A. Kraslawski, *Resour. Policy* 52, 81 <https://doi.org/10.1016/j.resourpol.2016.11.004> (2017).
- K. Goulding, T.S. Murrell, R.L. Mikkelsen, C. Rosolem, J. Johnston, H. Wang, and M.A. Alfaro, Outputs: potassium losses from agricultural systems, in *Improving potassium recommendations for agricultural crops*, vol 75. ed. by T.S. Murrell, R.L. Mikkelsen, G. Sulewski, R. Norton, and M.L. Thompson (Springer, Cham, 2021).
- W.O. Santos, E.M. Mattiello, L. Vergutz, and R.F. Costa, *J. Plant Nutr. Soil Sci.* 179, 547 <https://doi.org/10.1002/jpln.201500484> (2016).
- C.S. Rao and K. Srinivas, *Indian J. Fertil.* 13, 80 (2017).
- D. Das, B.S. Dwivedi, S.P. Datta, S.C. Datta, M.C. Meena, A.K. Dwivedi, M. Singh, D. Chakraborty, and S. Jaggi, *Geoderma* 393, 114983 <https://doi.org/10.1016/j.geoderma.2021.114983> (2021).
- S. Khan, R. Mulvaney, and T. Ellsworth, *Renew. Agric. Food Syst.* 29, 3 <https://doi.org/10.1017/S1742170513000318> (2014).
- T. Skorina and A. Allamore, *Green Chem.* 17, 2123 <https://doi.org/10.1039/C4GC02084G> (2015).
- S.S. Ibrahim, A.M. El Kammar, A.M. Guda, T.R. Boulos, and A. Saleh, *Part. Sci. Technol.* 37, 141 <https://doi.org/10.1080/02726351.2017.1376019> (2019).
- T.R. Choudhury, P.V. Raju, and T. Shaikh, *J. Geol. Soc. India* 98, 181 <https://doi.org/10.1007/s12594-022-1956-7> (2022).
- R.K. Tewatia, R.K. Rattan, S. Bhende, and L. Kumar, *Indian J. Fertil.* 13, 20 (2017).
- A.O. Shirale, B.P. Meena, P.P. Gurav, S. Srivastava, A.K. Biswas, J.K. Thakur, J. Somasundaram, A.K. Patra, and A.S. Rao, *J. Plant Nutr.* 42, 2682 <https://doi.org/10.1080/01904167.2019.1659353> (2019).
- R.A. Rawashdeh, *Resour. Policy* 69, 101834 <https://doi.org/10.1016/j.resourpol.2020.101834> (2020).
- N. Yakovleva, A.G. Chiwona, D.A.C. Manning, and O. Heidrich, *Resour. Policy* 74, 102426 <https://doi.org/10.1016/j.resourpol.2021.102426> (2021).
- D.A.C. Manning, *Agron. Sustain. Dev.* 30, 281 <https://doi.org/10.1051/agro/2009023> (2010).
- United State Geological Survey Potash, *Mineral Commodity Summaries*, (2022). <https://pubs.usgs.gov/periodicals/mcs2022/mcs2022-potash.pdf>.
- K. Majumdar, T.S. Murrell, S. Zingore, P. He, L. Prochnow, F. Gracia, S. Dutta and E. Francisco, In *Proceedings for the Frontiers of potassium Science Conference*, eds. T. S. Murrell, R.L. Mikkelsen. Peachtree Corners: International Plant Nutrition Institute (2017). Available online at: <http://KFrontiers.org>.
- P.J. White, M.J. Bell, I. Djalovic, P. Hinsinger, and Z. Rengel, Potassium use efficiency of plants, in *Improving potassium recommendations for agricultural crops*, vol 119. ed. by T.S. Murrell, R.L. Mikkelsen, G. Sulewski, R. Norton, and M.L. Thompson (Springer, Cham, 2021).
- D. Ciceri, M.D. Oliveira, R.M. Stokes, T. Skorina, and A. Allamore, *Min. Eng.* 102, 42 <https://doi.org/10.1016/j.mineng.2016.11.016> (2017).
- M. Rudmin, S. Banerjee, A. Mazurov, B. Makarov, and D. Martemyanov, *Appl. Clay Sci.* 150, 225 <https://doi.org/10.1016/j.clay.2017.09.035> (2017).
- S. Shekhar, V. Kumari, S. Sinha, D. Mishra, A. Agrawal, and K.K. Sahu, *Clays Clay Min.* 70, 135 <https://doi.org/10.1007/s42860-021-00171-4> (2022).
- A.B. Ghosh, *Bull. Indian Soc. Soil Sci.* 10, 317 (1976).
- D.A.C. Manning, *Proc. Geol. Assoc.* 126, 14 <https://doi.org/10.1016/j.pgeola.2014.12.005> (2015).
- C. Henderson, *Solids* 2, 1 <https://doi.org/10.3390/solids2010001> (2021).
- E. Karimi, A. Abdolzadeh, H.R. Sadeghipour, and A. Amineei, *Arch. Agron. Soil Sci.* 58, 983 <https://doi.org/10.1080/03650340.2011.557369> (2012).
- S. Shekhar, D. Mishra, A. Agrawal, and K.K. Sahu, *Appl. Clay Sci.* 143, 50 <https://doi.org/10.1016/j.clay.2017.03.016> (2017).
- C. Franzosi, L.N. Castro, and A.M. Celeda, *Natl. Resour. Res.* 23, 311 <https://doi.org/10.1007/s11053-014-9232-1> (2014).
- M. Rudmin, S. Banerjee, and B. Makarov, *Agronomy* 10, 872 <https://doi.org/10.3390/agronomy10060872> (2020).
- V. Baghel, J.K. Thakur, S.S. Yadav, M.C. Manna, A. Mandal, A.O. Shirale, P. Sharma, N.K. Sinha, M. Mohanty, and A.B. Singh, *Geomicrobiol J.* 37, 550 <https://doi.org/10.1080/01490451.2020.1734691> (2020).
- P.C. Matias, E.M. Mattiello, W.O. Santos, J.L. Badel, and V.H. Alvarez, *Min. Eng.* 132, 69 <https://doi.org/10.1016/j.mineng.2018.11.050> (2019).
- B.R. Rao, L.S. Rao, A.K. Mazumder, G.M. Rao, and T.C. Rao, *Min. Eng.* 6, 405 [https://doi.org/10.1016/0892-6875\(93\)90019-J](https://doi.org/10.1016/0892-6875(93)90019-J) (1993).
- V.P. Yadav, T. Sharma, and V.K. Saxena, *Int. J. Min. Process.* 60, 15 [https://doi.org/10.1016/S0301-7516\(99\)00083-6](https://doi.org/10.1016/S0301-7516(99)00083-6) (2000).
- A.M. Amer and N.K. Sediek, *Physicochem. Probl. Min. Process.* 37, 159 (2003).
- C.S. Rao and A.S. Rao, *Commun. Soil Sci. Plant Anal.* 30, 1105 <https://doi.org/10.1080/00103629909370271> (2008).
- W.O. Santos, E.M. Mattiello, L.M. da Costa, W.A.P. Abrahão, R.F. de Novais, and R.B. Cantarutti, *Int. J. Min. Process.* 140, 72 <https://doi.org/10.1016/j.minpro.2015.05.003> (2015).

39. R. Choudhury, A.T. Balagopal, and K.C. Banerjee, *Technology* 10, 128 (1973).
40. W.O. Santos, E.M. Mattiello, L.M. da Costa, A.A. Pacheco, L. Vergutz, L.F. Souza-Filho, and D.B. Abdala, *Int. J. Min. Process.* 159, 16 <https://doi.org/10.1016/j.minpro.2016.12.004> (2017).
41. Y. Pratap, H. Tanvar, and D. Moreira, *Min. Metall. Explor.* 37, 1231 <https://doi.org/10.1007/s42461-020-00218-5> (2020).
42. S. Shekhar, D. Mishra, A. Agrawal, and K.K. Sahu, *J. Clean. Prod.* 147, 681 <https://doi.org/10.1016/j.jclepro.2017.01.127> (2017).
43. S. Shekhar, S. Sinha, D. Mishra, A. Agrawal, and K.K. Sahu, *Sustain. Mater. Technol.* 23, e00129 <https://doi.org/10.1016/j.susmat.2019.e00129> (2020).
44. G. Nabi and W.K. Lu, *Ind. Eng. Chem. Fundam.* 13, 311 <https://doi.org/10.1021/i160052a003> (1974).
45. R.P. Viswanath, B. Viswanathan, and M.V.S. Satri, *React. Kinet. Catal. Lett.* 2, 51 <https://doi.org/10.1007/BF02060952> (1975).

Publisher's Note Springer Nature remains neutral with regard to jurisdictional claims in published maps and institutional affiliations.

Springer Nature or its licensor (e.g. a society or other partner) holds exclusive rights to this article under a publishing agreement with the author(s) or other rightsholder(s); author self-archiving of the accepted manuscript version of this article is solely governed by the terms of such publishing agreement and applicable law.